geoconvention
Calgary • Canada • May 7-11 2018

A Laboratory Acoustic Emission Experiment on Montney Shale

Suzie Jia[1], Ron Wong[1] and David Eaton[2]
[1] Department of Civil Engineering, University of Calgary, Email: qing.jia@ucalgary.ca
[2] Department of Geoscience, University of Calgary

Summary

A laboratory experiment has been conducted in which the evolution of wave velocities and stress-induced acoustic emission (AE) waveforms were recorded to investigate the progression of shear bands in Montney shale, which is characterized by transversely anisotropy. The wave velocities were used to 1) analyze the deformation-induced velocity anisotropy 2) construct velocity model improving hypocenter location accuracy. The P-wave first-arrivals were picked manually to invert three-dimensional AE source locations. This is the first AE test on a Montney shale specimen. Our results show that the peak strength of the sample is 290 MPa under a constant confining pressure of 10 MPa. Seismic velocities first increased significantly up to the initial crack closure stage, and then, increased gradually in the linear primary loading stage. In the post-peak stage, the sample exhibits strain-softening behaviour and the wave velocities decreased due to the creation of shear band. AE events were all triggered and recorded around the peak stress. Through hypocenter location analysis, a spatial correspondence of AE clusters and the shear band was found. Comparing with granite, the distinct characteristics of AE observation in Montney shale are: (1) in the uniform dilation stage, no AE event was recorded from Montney shale; (2) the AE signals have a lower signal-to-noise ratio; (3) the shear band developed in shale was scattered.

Introduction

The process of rock deformation can generate acoustic emissions (AEs) defined as transient elastic waves created by energy releases when (micro-)fractures are undergoing inelastic deformations inside a material (Lockner, 1993). AEs are analogous to natural earthquakes as they exhibit similar source mechanisms with seismic events recorded in the field, but in different scales: AEs have higher frequencies (>10 kHz) and smaller magnitudes (Bohnhoff et al., 2010; Goodfellow et al., 2015). As the AE tests can be conducted under arbitrarily controlled conditions, the observed data enables us to gain insight into fracture nucleation and evolution processes (Lockner et al., 1991).

A wide range of studies have been carried out towards AE data analysis across various disciplines, from mining to aerospace engineering. In rock mechanics, previous AE tests were mainly conducted on granites or sandstones, which can store sufficient energy before mobilization for AE event detection (Lockner et al., 1991; Lockner, 1993; Reches and Lockner, 1994; Thompson et al., 2009). However, there are no published systematic AE investigations (e.g., source location, moment tensor inversion, etc.) on Montney shale. Numerous studies have revealed that the presence of clay minerals can significantly weaken fault frictional strengths, and fault gouges primarily consist of montmorillonite, illite and chlorite implying a potentially low seismic radiated energy (Shimamoto and Logan, 1981). Thus, it remains a challenge to investigate the failure behavior of shale through quantitative AE data analysis.

In this study, a conventional triaxial compression (TC) test was conducted while AE data were recorded simultaneously. The experimental details are first introduced including rock samples, experimental

apparatus, and loading procedure. The preliminary results on the TC test are then presented with emphasis on mechanical data, variations of ultrasonic P wave velocities and event hypocenter locations.

Experimental Details

Montney shale was chosen because it has a relatively high strength compared with other shales and it has emerged as one of the most popular unconventional hydrocarbon plays in Canada. The Montney sample for this test was cored by Seven Generations Ltd from a vertical well (UWI: 00/13-28-064-05 W6M) at the depth of 3136.50 m located in the Kakwa area. Previous test results indicate those samples have peak strengths of $~300 MPa$ under a confining pressure of 15 MPa (Young's modulus is around 50 GPa) showing considerably weak anisotropy (both ε and γ are < 0.01) (Thomsen, 1986; McKean, 2017). The μCT scan shows the test sample is homogeneous without significant lamination feature except for some light spots indicating a higher density, which may generate stiffness contrast, and thus inducing high stress concentrations around some areas resulting in a premature failure.

The cylindrical sample of 125.8 mm in length and 50.29 mm in diameter (2:5 length/diameter aspect ratio) was prepared following the International Society of Rock Mechanics standard. This experiment was conducted in a triaxial geophysical imaging cell (GICA cell) where the axial load was delivered by the MTS axial hydraulic actuator and the confining pressure was maintained by silicone oil outside of a rubber confining jacket using a servo-control Teledyne system. Two linear variable differential transformers (LVDTs) measured axial deformation.

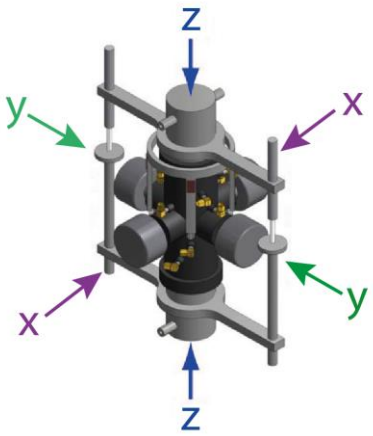

Figure 1. The triaxial geophysical imaging cell is equipped with AE transducers (yellow) and ultrasonic transducers located along three orthogonal axes (*x, y, z*). Modified from Goodfellow et al. (2014).

Sixteen piezoelectric transducers were used for passive monitoring of the high frequency AE signals emitted from the sample as it was compressed, which formed a good coverage around the specimen for moment tensor inversions. Each of these AE sensors had a calibrated frequency of 200 KHz to 1 MHz. To aid in the source location analysis (Lockner et al., 1991), three pairs of dedicated ultrasonic transducers measuring compressional wave (P) and two polarized shear waves velocities were located along three orthogonal axes in the cell to conduct velocity surveys (Figure 1). After the experiment, the continuous acoustic emission waveforms were harvested and extracted for discrete AE events with a triggering threshold voltage of 80 mV recorded at least four channels.

The sample was deformed under a constant confining pressure of 10 MPa. The triaxial system was first gradually loaded to 10MPa hydrostatic pressure under load control. Then the MTS axial actuator was held under constant displacement control mode with a rate of 0.2 μm/s. For every increment of 5 to 10 MPa in the axial stress, attempts were made to carry out ultrasonic wave velocity measurements once the system

started loading. As the AE sensors cannot send and receive signal at the same time, no seismic survey was made when the sample was close to failure.

Results

Geomechanical Data

The stress-strain curve of this test is shown in Fig. 2. The hydrostatic loading part of the test is shown in the curve up to Point A, and after that, the deviatoric stress starts to increase. Portion A to B has a significantly low slope indicating the closure of pre-existing micro-cracks, which could be induced by stress relaxation. For portion B to C, the sample displays a linear primary loading curve (potentially elastic behaviour). Point C is the onset of crack initiations, where the curve begins to slightly deviate from linearity, and plastic deformation begins. From Point D, the curve starts to curve indicating permanent axial deformations as defined by Martin (1997).

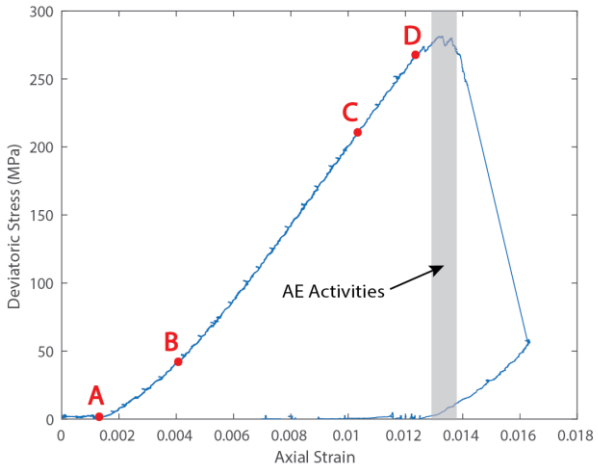

Figure 2. The stress-strain curve.

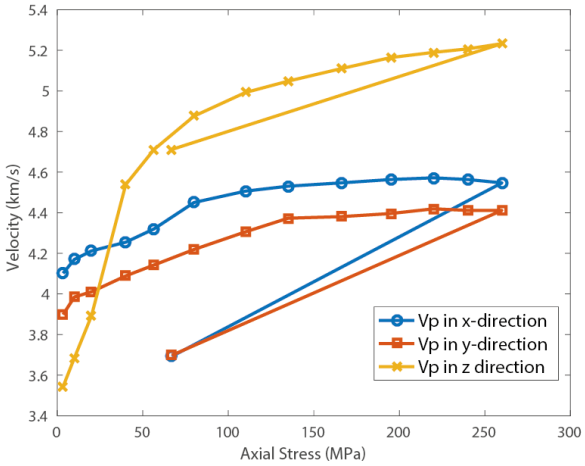

Figure 3. P wave velocities in three directions.

Once the stress condition reaches the peak at a deviatoric stress and axial strain of roughly 280 MPa and 1.3% respectively, the sample undergoes an unstable failure process with significant strain-softening. A shear band was formed after the test showing an inclination angle of 70º with respect to the axial stress, which does not follow the typical orientation of shear deformation defined by Mohr-Coulomb (i.e., $45º+\phi/2$).

One postulation for this phenomenon is that the shear band mainly consists of axial cracks normal to the confining pressure and connected by bedding-parallel side-steps under low confining pressure, thus leading to a shear-dilation behaviour (Niandou et al., 1997; Amann et al., 2012). Based on the linear portion of the stress-strain curve, the static Young's Modulus E is about 28 GPa, and the residual frictional strength is 67 MPa.

Elastic Wave Velocities

Fig. 3 illustrates the P-wave velocities in three orthogonal axes. Note the initial velocity in the z-axis is significantly lower than the other two, and Vp in the x direction travels faster than that in the y direction, which indicates inclined bedding planes with bed normal axes deviated slightly from the z axis towards the y axis. The velocity increase is fastest in the axial direction before the onset of linear primary loading ($\sigma1$ = 40 MPa). In the post-peak, velocities in the x and y directions decrease more significantly than that in the z-axis confirming that stress-induced cracks are mainly formed normal to the x-y plane.

AE Event Hypocenters

The AE sensors detected more than 300 AE events of which 191 events were located. The quality of the AE data was mainly based on the signal to noise ratio. Unlike granite, the waveforms generated from Montney Shale did not always show a clear first arrival making the picking process quite challenging. Fig. 4 displays AE locations in five time intervals, and each contains a time period of 0.33 s. Note that all events occurred around the peak as indicated by shaded time zone in the stress-strain curve (Fig. 2). Each event was colored by its corresponding moment magnitude.

The nucleation process was started from the upper side of the sample as illustrated in time interval 1 (T1) in Fig. 4. Then the AE cluster expanded from the top to the bottom forming a band (T2 to T5) crosscutting the sample, which was in agreement of the observations of shear band. The progression of failure in the Montney Shale was notably different from that in granite: the AE cluster formed after crack nucleation in Montney Shale was quite scattered; whereas, for granite, the cluster was more linear. The two possible explanations are: (1) the material is weakly anisotropic, so that the bedding planes can affect the orientation of fracture growth, especially under low confining pressure (Niandou et al., 1997); (2) the high-density grains can influence stress distributions and strain localization processes.

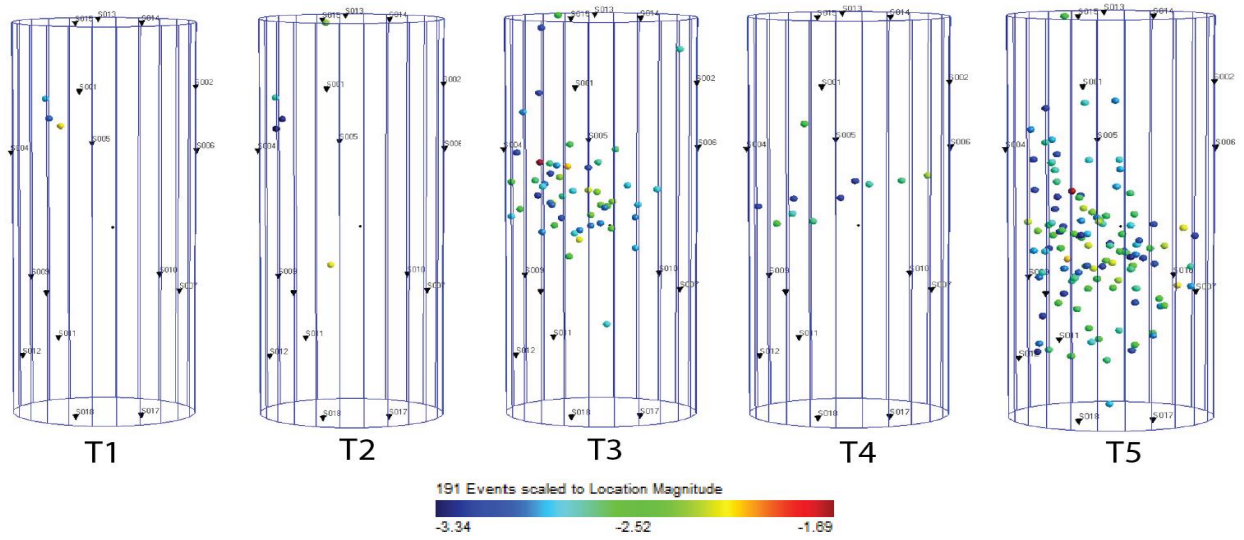

Figure 4. AE hypocenter distribution in five time intervals. Each time interval had a period of 0.33s. The dot colors corresponded to their moment magnitudes. All events occurred in the shaded time slot indicated in Fig. 2.

Conclusions

The differences in terms of AE activities between granite (using the tests carried out by \cite{Lockner91}) and Montney Shale under conventional triaxial compression tests can be summarized as: (1) AE events occurred throughout the center part of granite when it undergoes uniform dilation stage; whereas, for Montney Shale, no AE was detected until it nearly reached the peak; (2) AE signals from granite showed a higher signal-to-noise ratio than that of Montney Shale; (3) The shear band in granite was linear and clean; on the other hand, the shear band was scattered in Montney Shale.

Acknowledgements

Sponsors of the Microseismic Industry Consortium are sincerely thanked for their support of this initiative. This work was supported by funding to Dr. David Eaton for the NSERC/Chevron Industrial Research Chair in Microseismic System Dynamics. The authors would like to thank Dr. Jeffery Priest and Scott McKean for sample preparations, Dr. Paul Young and Dr. Farzine Nasseri for helping with the experimental work. Itasca is also thanked for providing InSite software to process the AE dataset.

References

Amann, F., P. Kaiser, and E.A. Button, 2012, Experimental Study of Brittle Behavior of Clay Shale in Rapid Triaxial Compression: Rock Mechanics and Rock Engineering, 45(1), 21-33.

Bohnhoff, M., G. Dresen, W.L. Ellsworth, and H. Ito, 2010, Passive Seismic Monitoring of Natural and Induced Earthquakes: Case Studies, Future Directions and Socio-Economic Relevance: In: S. Cloetingh, J. Negendank (eds.), New Frontiers in Integrated Solid Earth Sci., Int. Yr. Planet Earth, Springer.

Goodfellow, S.D., J.W. Flynn, J.M. Reyes-Montes, M.H.B. Nasseri, and R.P. Young, 2014, Acquisition of Complete Acoustic Emission Amplitude Records during Rock Fracture Experiments: Journal of Acoustic Emission, 32, 1-11.

Goodfellow, S.D., M H.B. Nasseri, S.C. Maxwell, and R.P. Young, 2015, Hydraulic Fracture Energy Budget: Insights from the Laboratory: Geophys. Res. Lett., 42, 3179-3187.

Goodfellow, S.D., B. Lee, W. Flynn, S.C. Maxwell, M.H.B. Nasseri, R.P. Young, and L.E.A. Lombos, 2016, Acoustic Emission Geomechanics of Hydraulic Fracturing in the Laboratory: American Rock Mechanics Association, Houston, Texas.

Lockner, D., J.D. Byerlee, V. Kuksenko, A. Ponomarev, and A. Sidorin, 1991, Quasi-static Fault Growth and Shear Fracture Energy in Granite: Nature, Vol. 350, No. 6313, pp. 39-42, 7th March.

Lockner, D., 1993, The Role of Acoustic Emission in the Study of Rock Fracture: Int. J. Rock Mech. Min. Sci. and Geomech. Abstr., Vol. 30, No. 7, pp. 883-899.

McKean, S., 2017, Geomechanical Properties of the Montney and Sulphur Mountain Formations: Master Thesis, University of Calgary.

Martin, C.D., 1997, Seventeenth Canadian Geotechnical Colloquium: The Effect of Cohesion Loss and Stress Path on Brittle Rock Strength: Canadian Geotechnical Journal, 34(5), 698-725.

Niandou, H., J.F. Shao, J.P. Henry, and D. Fourmaintraux, 1997, Laboratory Investigation of the Mechanical Behaviour of Tournemire Shale: International Journal of Rock Mechanics and Mining Sciences, 34(1), 3-16.

Reches, Z., and D.A. Lockner, 1994, Nucleation and growth of faults in brittle rocks: J. Geophys. Res., 99(B9), 18159-18173

Shimamoto, T., and J.M. Logan, 1981, Effects of simulated clay gouges on the sliding behavior of Tennessee sandstone: Tectonophysics, 75, 243-255.

Thomsen, L., 1986, Weak Elastic Anisotropy: Geophysics, 51(10), 1954-1966.

Thompson, B.D., R.P. Young, and D.A Lockner, 2009, Premonitory Acoustic Emissions and Stick-slip in Natural and Smooth-faulted Westerly Granite: J. Geophys. Res., 114, B02202.